

New Early Dark Energy is compatible with current LSS data

Florian Niedermann* and Martin S. Sloth†

CP³-Origins, Center for Cosmology and Particle Physics Phenomenology

University of Southern Denmark, Campusvej 55, 5230 Odense M, Denmark

Recently a full-shape analysis of Large-Scale Structure (LSS) data was employed to provide new constraints on a class of Early Dark Energy (EDE) models. In this note we derive similar constraints on New Early Dark Energy (NEDE) using the publicly available `PyBird` code. Including the full-shape analysis of LSS together with measurements of the Cosmic Microwave Background (CMB), Baryonic Acoustic Oscillations (BAO) and supernovae (SN) data, we report $H_0 = 71.2 \pm 1.0 \text{ km s}^{-1} \text{ Mpc}^{-1}$ (68% C.L.) together with a $\simeq 4\sigma$ evidence for a non-vanishing fraction of NEDE. This is an insignificant change to the value previously found without full-shape LSS data, $H_0 = 71.4 \pm 1.0 \text{ km s}^{-1} \text{ Mpc}^{-1}$ (68% C.L.). As a result, NEDE is compatible with current constraints from LSS data.

PACS numbers: 98.80.Cq,98.80.-k,98.80.Es

* niedermann@cp3.sdu.dk

† sloth@cp3.sdu.dk

I. INTRODUCTION

Recent direct measurements of the expansion rate of the universe using Type Ia SN as standard candles (SH0ES [1]) or strong gravitational lensing (H0LiCOW [2]) are in tension with the expansion rate inferred from the CMB [3] when assuming the standard Λ CDM cosmological model (for recent reviews see [4–7]). It is a hot subject of discussion whether unaccounted for systematic effects in astronomical distance measurements are responsible for this discrepancy or whether we have to refine our understanding of the history of the universe by going beyond the Λ CDM model [8, 9]. It turns out that cosmological measurements have reached a precision where modifying the history of the universe to bring new concordance between CMB and direct measurements of the expansion rate is very difficult without introducing new tensions between different data sets. As theorists looking for a new concordance model to replace Λ CDM, we are truly experiencing that we have entered the era of precision cosmology. If we try to modify the late time history to account for the higher value of H_0 measured today by SH0ES and H0LiCOW, then we quickly run into tension with BAO measurements [4, 5, 10–12]. On the other hand, an extra component of dark energy, which decays away shortly before recombination has proved more promising as a possible solution [13–21]. The Early Dark Energy (EDE) proposal suggests that the early dark energy is stored in a slow-rolling scalar field and decays away as the scalar field approaches the bottom of its potential and picks up speed, similar to how inflation ends in slow-roll inflation. However, in order to satisfy phenomenological constraints the potential has to be relatively fine-tuned. But more seriously, recent fits including a full-shape analysis of LSS data have challenged the ability of EDE to solve the Hubble tension at all [22–24].

Many of the issues with EDE are avoided in the more recent New Early Dark Energy (NEDE) proposal [25, 26]. Here, the early dark energy decays away in a first order phase transition, and the free energy released is partially converted into small-scale anisotropic stress (behaving similar to a stiff fluid on large scales) and gravitational radiation, which provides a good fit to all cosmological data, including the recent measurements of H_0 by SH0ES and H0LiCOW. It remains however to be seen what a full-shape analysis of LSS data will imply for NEDE to serve as a new concordance model. The purpose of this short note is to provide such an analysis.

The full-shape analysis of the matter power spectrum within EDE was carried out in [23] and [27] us-

ing the Effective Field Theory of Large-Scale Structure¹ (EFTofLSS) applied to BOSS/SDSS data [24, 50, 51]. In particular, in [27] the code `PyBird` was used for the full-shape analysis of LSS data and also made public by the same collaboration. This has enabled us to use the same code to repeat their analysis for NEDE. We therefore employ `PyBird` to analyze the full-shape of the LSS power spectrum, and use it alongside CMB, (small- z and large- z) BAO and supernovae data to constrain NEDE. We have tested our implementation of it on Λ CDM and w CDM where we find agreement with [27] and [52], respectively.

Below we will provide a short review of the NEDE model, following [25, 26], and then discuss the data analysis and results.

II. NEW EARLY DARK ENERGY

NEDE is associated with the false vacuum energy of a two-component scalar field (ψ, ϕ) that undergoes a first order phase transition. The corresponding potential reads²

$$V(\psi, \phi) = \frac{\lambda}{4} \psi^4 + \frac{1}{2} M^2 \psi^2 - \frac{1}{3} \alpha M \psi^3 + \frac{1}{2} m^2 \phi^2 + \frac{1}{2} \tilde{\lambda} \phi^2 \psi^2, \quad (\text{II.1})$$

where the parameters λ , $\tilde{\lambda}$ and α are positive and dimensionless, and we assume that $\lambda/\alpha^2 < 1/4$ for the potential to have a non-trivial vacuum structure. In particular, the true vacuum corresponds to $(\psi, \phi)_{\text{True}} = \left(\frac{M}{2\lambda} \left[\alpha + \sqrt{\alpha^2 - 4\lambda} \right], 0 \right)$. With these definitions, the NEDE background energy density is $\bar{\rho}_{\text{NEDE}} = V(\psi_{\text{False}}, \phi(t)) - V(\psi_{\text{True}}, 0)$, corresponding to a fraction of the total energy density $\bar{\rho}$ given by $f_{\text{NEDE}} = \bar{\rho}_{\text{NEDE}}(t_*)/\bar{\rho}(t_*)$, where t_* is the time of the phase transition. This additional energy component then leads to an increase in the Hubble parameter, $H(t)$, prior to recombination, which in turn reduces the comoving sound horizon $r_s(z_{\text{rec}}) = \int_{z_{\text{rec}}}^{\infty} dz v(z)/H(z)$, with $v(z)$ denoting the sound speed in the photon-baryon fluid. This alone would shift the angular position of the first peak in the CMB power spectrum, $\theta_{\text{rec}} = r_s(z_{\text{rec}})/D_{\text{rec}}$, which is highly constrained. The change in $r_s(z_{\text{rec}})$ is, however, compensated by simultaneously lowering the comoving distance to the surface of last scattering, D_{rec} , such that θ_{rec} remains unchanged. As $D_{\text{rec}} \propto 1/H_0$, this is achieved by an increase in the Hubble parameter H_0 , which at the same time resolves the tension between its local

¹ The EFTofLSS was first formulated in [28–30] and later used to compute the dark matter power spectrum [31–43].

An IR-resummed version of the EFTofLSS was then able to reproduce the BAO peak [44–49]. For a more complete account of all related research see for example the references provided in [24].

² As compared to [26], we have set $\beta = 1$ which can always be achieved by rescaling M .

and CMB inferred value. For this mechanism to work, it is crucial that the NEDE energy component decays around recombination to avoid over-closing the universe. In our case this decay is triggered by the ultralight scalar field $\phi(t)$. It traces an almost flat direction in field space, corresponding to the mass scale $m \sim 10^{-27} \text{eV}$, whereas ψ has a much heavier mass, $M \sim 0.1 \text{eV} \gg m$, setting the scale of NEDE. This huge hierarchy can be stabilized against quantum corrections by imposing [26] $\tilde{\lambda} < \mathcal{O}(1) \times 10^3 m^2/M^2$. Initially, the field is frozen due to the Hubble friction and prevented from tunneling to the true minimum by a high potential barrier in ψ direction, explicitly $(\psi, \phi)_{\text{ini}} = (0, \phi_{\text{ini}}) \simeq \text{const}$. Once the Hubble drag gets released, ϕ starts rolling, thereby decreasing the potential barrier ‘seen’ by ψ and triggering the phase transition. This happens within one Hubble time and before ϕ reaches its minimum. The exact timing depends on the details of the potential, but falls in the range³ $0.18 < H(t_*)/m < \mathcal{O}(1)$, where the decay time t_* is implicitly determined through the ‘trigger parameter’ $H(t_*)/m$. The lower bound corresponds to the point of maximal tunneling probability (when ϕ crosses zero for the first time) and the upper bound ensures that the Hubble drag has been released. For $\alpha = \mathcal{O}(1)$ the tunneling rate is $\Gamma(t) \sim M^4 e^{-S_E(t)}$, where $S_E(t)$ is the Euclidian action evaluated at the ‘bounce solution’. Its time dependence is inherited from the trigger field $\phi(t)$ that scans the potential. The inverse duration of the phase transition $\bar{\beta} \simeq \dot{\Gamma}/\Gamma$ (approximating $\Gamma \propto e^{\bar{\beta}t}$) was then found to be [26]

$$H(t_*)\bar{\beta}^{-1} = \mathcal{O}(1) \times 10^{-3} \left(\frac{f_{\text{NEDE}}}{0.1} \right)^{1/2} (11\alpha^2/9 - 1)^{-1/2} \left(\frac{M_{\text{pl}}/\phi_{\text{ini}}}{10^4} \right) \left(\frac{H(t_*)/m}{0.2} \right) \left(\frac{\lambda}{0.01} \right)^{3/2}, \quad (\text{II.2})$$

provided $\tilde{\lambda}$ saturates its naturalness bounds and the quartic coupling is sufficiently weak, $\lambda < 0.02$. Here, we used that $S_E(t_*) \simeq 250$ which follows from the percolation condition $\Gamma(t_*)/H^4 \gtrsim 1$, which is fulfilled when bubble nucleation becomes efficient, i.e. there is more than one nucleation event per Hubble time and volume. For the above suggested parameter choices, we therefore find that the phase transition happens on a time scale that is short compared to the Hubble expansion. After the transition, the space is filled with a condensate of colliding bubble walls. This state is dominated by small-scale anisotropic stress and expected to behave on large scales like a fluid dominated by kinetic rather than potential energy, and therefore it decays quicker than radiation. As a result, our microscopic model can be described in terms of an effective cosmological fluid, dubbed NEDE fluid,

³ As argued in [26], the upper bound tightens to $\lesssim 0.21$ when suppressing oscillations of ϕ around the true vacuum.

which first (before t_*) behaves like vacuum energy but then (after t_*) redshifts away with an equation of state parameter $w_{\text{NEDE}}(t) > 1/3$. A priori, w_{NEDE} is time-dependent, but we will approximate it as a constant. This is justified because NEDE can impact cosmological observables only in a short redshift window around its decay time; explicitly, we take

$$w_{\text{NEDE}}(t) = \begin{cases} -1 & \text{for } t < t_* , \\ w_{\text{NEDE}}(t_*) & \text{for } t \geq t_* . \end{cases} \quad (\text{II.3})$$

At the background level, NEDE is therefore described in terms of four parameters, the fraction of NEDE at decay time, f_{NEDE} , the mass of the trigger field, m , the trigger parameter, $H(t_*)/m$ (which together with m fixes the decay redshift z_*), and the equation of state of the NEDE fluid right after percolation has been completed, $w_{\text{NEDE}}(t^*)$. Perturbations in the NEDE fluid are generated after the phase transition. They arise from adiabatic perturbations of the trigger field, $\delta\phi(t, \mathbf{x})$, which cause spatial variations of the decay time. The NEDE density contrast and velocity divergence as a function of k right after the decay are [26]

$$\delta_{\text{NEDE}}(t_*, k) = -3 [1 + w_{\text{NEDE}}(t_*)] H(t_*) \frac{\delta\phi(t_*, k)}{\dot{\phi}(t_*)} , \quad (\text{II.4a})$$

$$\theta_{\text{NEDE}}(t_*, k) = \frac{k^2}{a(t_*)} \frac{\delta\phi(t_*, k)}{\dot{\phi}(t_*)} . \quad (\text{II.4b})$$

These initial values are then propagated forward in time using the adiabatic perturbation equations of a generic fluid [53].

III. DATA ANALYSIS AND RESULTS

We use the publicly available code `TriggerCLASS`⁴ [26], which implements NEDE in the Boltzmann code `CLASS` (Cosmic Linear Anisotropic Solving System) [54]. We then scan the cosmological parameters with the Monte Carlo Markov Chain (MCMC) code `MontePython` [55, 56], employing the Metropolis-Hastings algorithm. To that end, we impose flat priors with standard ranges on the dimensionless baryon and cold dark matter density, ω_b and ω_{cdm} , the Hubble parameter H_0 , the amplitude of primordial curvature perturbations at $k = 0.05 \text{ Mpc}^{-1}$, $\ln 10^{10} A_s$, the spectral tilt, n_s , and the reionization optical depth, τ_{reio} . In keeping with the Planck convention, the neutrino sector contains

⁴ <https://github.com/flo1984/TriggerCLASS>

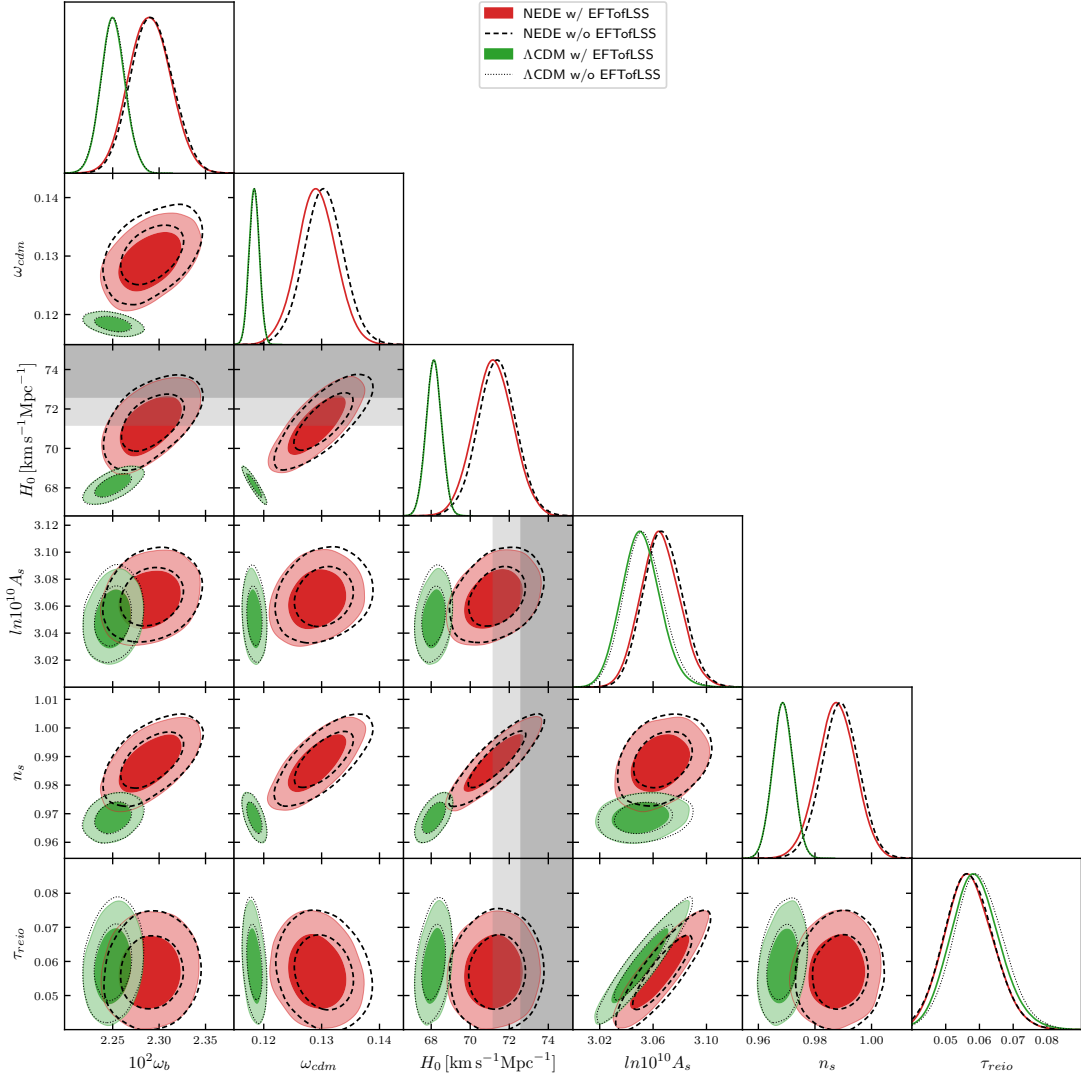


FIG. 1. Posteriors and covariances of standard cosmological parameters for Λ CDM (green) and NEDE (red). The result of the combined analysis without EFTofLSS corresponds to the dashed (NEDE) and dotted (Λ CDM) contours. Here and henceforth, the 68% C.L. and the 95% C.L. correspond to the darker and lighter shaded regions, respectively. The gray band corresponds to the SH₀ES constraint on H_0 . Overall, including EFTofLSS has a negligible effect.

two massless and one massive species with $M_\nu = 0.06$ eV, where the effective number of relativistic degrees of freedom is fixed to $N_{\text{eff}} = 3.046$. Alongside these standard parameters, we also vary the trigger mass through $\log_{10}(m/m_0)$ (where $m_0 = 1/\text{Mpc}$) and the NEDE fraction f_{NEDE} . We impose flat priors with ranges $1.3 < \log_{10}(m/m_0) < 3.3$ and $0 < f_{\text{NEDE}} < 0.3$. Λ CDM is recovered for $f_{\text{NEDE}} = 0$.

For our base model we further fix $H(t_*)/m = 0.2$ and choose $w_{\text{NEDE}}(t_*) = 2/3$ in accordance with having an admixture of a stiff fluid.⁵ The perturbation sector assumes a rest-frame sound speed that equals the adiabatic sound speed and a vanishing viscosity parameter (as defined in [57]).

In all our runs we include the following data sets: The Planck 2018 TT, TE, EE and lensing likelihood with the full set of nuisance parameters [58], supernovae data from the combined Pantheon sample [59], the locally measured value $H_0 = 74.03 \pm 1.42 \text{ km s}^{-1} \text{ Mpc}^{-1}$ (68% C.L.) from SH₀ES [1] implemented as a Gaussian prior, the primordial Helium abundance $Y_p = 0.2449 \pm 0.0040$ (68% C.L.) from [60] and the small- z BAO measurements of the SDDS DR7 main Galaxy sample [61] and the 6dF Galaxy Survey [62] at redshifts $z = 0.15$ and $z = 0.106$, respectively. With regard to any additional data set, we distinguish two different analyses:

1. Combined analysis **without EFTofLSS**: High- z BAO measurements together with constraints on $f\sigma_8$, quantifying the growth of structure, obtained from the CMASS and LOWZ galaxy samples of BOSS DR 12 [63] at redshifts $z = 0.38, 0.51, 0.61$. This run does not capture the full shape of the matter power spectrum (it merely contains some condensed information through $f\sigma_8$).
2. Combined analysis **with EFTofLSS**: Here, we include the EFTofLSS applied to the BOSS/SDDS sample [24, 50, 51]. It contains the full-shape information on the galaxy power spectra obtained from the sky-cuts CMASS NGC, CMASS SGC and LOWZ NGC at the effective redshifts $z = 0.57$ (CMASS) and $z = 0.32$ (LOWZ). This is combined with constraints on BAO parameters measured from the same samples using the post-reconstructed power spectra and taking into account the covariance among all data sets. The full-shape and BAO data together with their covariances are implemented via the MontePython likelihood extension PyBird⁶.

For each data set combination we run both the Λ CDM and our NEDE base model using between 8 and 16 chains. We consider chains to be converged if the Gelman-Rubin criterion [64] fulfills $R - 1 < 0.01$. Especially in the case of NEDE, this requires a rather large number of total steps of the order 3×10^6 . As we find, this is vital to deriving well-converged uncertainties for f_{NEDE} , needed to make a reliable statement about the statistical evidence for NEDE. The exact convergence

⁵ For extended runs where either parameter is allowed to vary see [26].

⁶ <https://github.com/pierrexyz/pybird.git>

Parameter	Λ CDM		NEDE	
	w/o EFTofLSS	w/ EFTofLSS	w/o EFTofLSS	w/ EFTofLSS
$100 \omega_b$	$2.251^{+0.014}_{-0.013}$ (2.251)	$2.250^{+0.013}_{-0.014}$ (2.256)	$2.292^{+0.022}_{-0.024}$ (2.297)	$2.290^{+0.022}_{-0.023}$ (2.288)
ω_{cdm}	$0.1184^{+0.0009}_{-0.0009}$ (0.1183)	$0.1183^{+0.0009}_{-0.0009}$ (0.1181)	$0.1304^{+0.0034}_{-0.0035}$ (0.1306)	$0.1291^{+0.0033}_{-0.0034}$ (0.1295)
$H_0 [\text{km s}^{-1} \text{Mpc}^{-1}]$	$68.13^{+0.41}_{-0.41}$ (68.16)	$68.14^{+0.40}_{-0.41}$ (68.31)	$71.4^{+1.0}_{-1.0}$ (71.5)	$71.2^{+1.0}_{-1.0}$ (71.28)
$ln10^{10} A_s$	$3.053^{+0.014}_{-0.016}$ (3.053)	$3.051^{+0.014}_{-0.015}$ (3.049)	$3.067^{+0.014}_{-0.015}$ (3.068)	$3.065^{+0.014}_{-0.015}$ (3.064)
n_s	$0.9686^{+0.0037}_{-0.0037}$ (0.9698)	$0.9686^{+0.0037}_{-0.0037}$ (0.9696)	$0.9889^{+0.0067}_{-0.0066}$ (0.9912)	$0.9876^{+0.0070}_{-0.0066}$ (0.9884)
τ_{reio}	$0.0599^{+0.0071}_{-0.0078}$ (0.0598)	$0.0589^{+0.0068}_{-0.0078}$ (0.0573)	$0.0571^{+0.0068}_{-0.0077}$ (0.0572)	$0.0571^{+0.0068}_{-0.0077}$ (0.0557)
f_{NEDE}	–	–	$0.126^{+0.032}_{-0.029}$ (0.1296)	$0.117^{+0.033}_{-0.030}$ (0.120)
$\log_{10}(m/m_0)$	–	–	$2.56^{+0.12}_{-0.10}$ (2.57)	$2.55^{+0.12}_{-0.11}$ (2.53)
σ_8	$0.8090^{+0.0060}_{-0.0065}$ (0.8092)	$0.8080^{+0.0058}_{-0.0063}$ (0.8064)	$0.841^{+0.010}_{-0.010}$ (0.841)	$0.836^{+0.010}_{-0.010}$ (0.837)
S_8	$0.814^{+0.010}_{-0.010}$	$0.813^{+0.010}_{-0.010}$	$0.841^{+0.012}_{-0.012}$	$0.836^{+0.012}_{-0.012}$
$r_s^d [\text{Mpc}]$	$147.40^{+0.23}_{-0.23}$ (147.38)	$147.40^{+0.23}_{-0.23}$ (147.39)	$141.0^{+1.6}_{-1.7}$ (140.9)	$141.6^{+1.6}_{-1.7}$ (141.4)
z_*	–	–	4920^{+620}_{-730} (4960)	4900^{+660}_{-800} (4720)
$\Delta\chi^2$	0	0	-15.6	-14.7
$f_{\text{NEDE}} \neq 0$	–	–	4.3σ	3.9σ
$10^3 \times \max(R-1)$	2.1	2.7	7.8	3.3

TABLE I. The mean value and $\pm 1\sigma$ error (with bestfit value in parentheses) of the cosmological parameters from our combined analyses for Λ CDM and NEDE with and without EFTofLSS.

values are detailed in Tab. I. As initial covariance matrices we use the ones from the respective Λ CDM runs, which are then updated through `MontePython`'s 'superupdate' option. We also tested our data pipeline, including its `PyBird` implementation, by reproducing different results obtained in [52] in the case of w CDM.⁷

A detailed discussion of NEDE and its phenomenology has been provided in [26]. Here, we will therefore limit ourselves to a quick review of the main phenomenological features of NEDE and rather focus on the impact additional LSS data has on the extracted parameter values. As mentioned before, the primary effect of NEDE is to lower the sound horizon. This then needs to be balanced by increasing H_0 in order to reduce the comoving distance between us and the surface of last scattering. This can be seen in Fig. 2, which shows an (approximate) degeneracy between H_0 and the sound horizon at radiation drag r_s^d . As a result, the NEDE contour (w/ and w/o EFTofLSS) largely overlaps with the gray band representing the SH₀ES measurement, thereby resolving the Hubble tension. Another

⁷ Specifically, we checked that we agree with the results of the MCMC analyses performed with the data set combinations 'BAO + FS', 'BAO + FS w/o Ly- α ', 'CMB + BAO' and 'CMB + FS + BAO'.

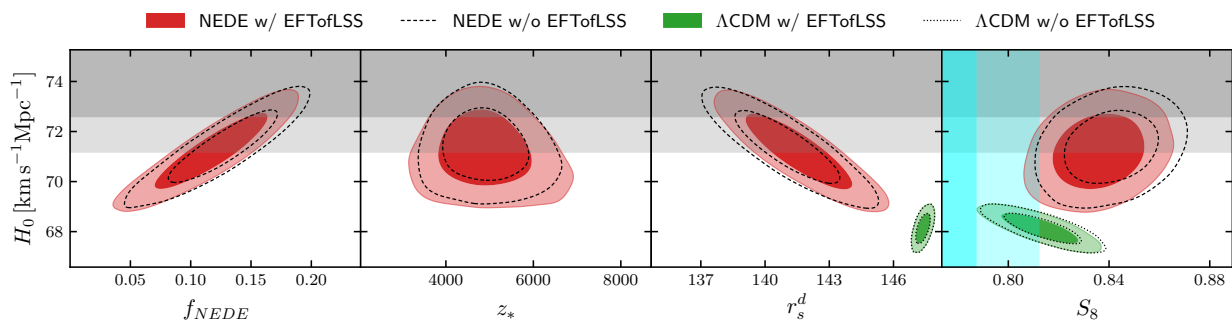


FIG. 2. Covariances of H_0 vs a subset of parameters for the combined analysis with (red and green filled contour) and without (dashed and dotted contour) EFTofLSS. A recent constraint on S_8 from weak gravitational lensing [65] is depicted by the light blue band. The gray band represents the recent SH₀ES measurement. The change in f_{NEDE} when including EFTofLSS is insignificant.

important effect of NEDE, which is especially relevant for LSS, is its positive correlation with the (dimensionless) dark matter energy density ω_{cdm} , which can for example be inferred from the H_0 vs w_{cdm} plot in Fig. 1. The physical reason for this has been discussed in the context of acoustic dark energy [16], but applies equally to NEDE: oscillations in the NEDE fluid cause a stronger overall decay of the Weyl potential, which needs to be compensated by increasing ω_{cdm} . Finally, EDE type models are known to enhance the diffusion damping on small scales. This corresponds to a loss of power which can be counteracted by reducing the spectral tilt (or $n_s \rightarrow 1$ equivalently). In fact, from Fig. 1 we infer that n_s becomes 2σ compatible with a scale invariant spectrum.

Here, we ask whether this picture is adversely affected by including additional LSS data as recently claimed in the context of the old EDE proposal [23, 27]. The short answer is that this is not the case. Including additional LSS data only leads to an insignificant change of previous results without the EFTofLSS data set. This is obvious from comparing the red (w/ EFTofLSS) and dashed contours (w/o EFTofLSS) in Fig. 1 and 2, which are almost identical. On a more quantitative level, we report a small reduction of the preferred amount of NEDE as detailed in Tab. I. Without including the EFTofLSS, we have $f_{\text{NEDE}} = 12.6^{+3.2}_{-2.9}\%$ which corresponds to a 4.3σ evidence for a non-vanishing NEDE parameter and an increased Hubble parameter of $H_0 = 71.4 \pm 1.0 \text{ km s}^{-1} \text{ Mpc}^{-1}$. These values undergo small insignificant ($< 0.5\sigma$) changes when we include the EFTofLSS, specifically $f_{\text{NEDE}} = 11.7^{+3.3}_{-3.0}\%$ and $H_0 = 71.2 \pm 1.0 \text{ km s}^{-1} \text{ Mpc}^{-1}$, corresponding to a (still large) 3.9σ evidence for NEDE. With regard

Dataset	Λ CDM		NEDE			
	w/o	w/	w/o		w/	
	χ^2	χ^2	χ^2	$\Delta\chi^2$	χ^2	$\Delta\chi^2$
<i>Planck</i> high- ℓ TT, TE, EE	2,348.9	2351.1	2,348.2	-0.8	2348.2	-2.9
<i>Planck</i> low- ℓ TT	22.7	22.6	20.8	-1.9	21.0	-1.6
<i>Planck</i> low- ℓ EE	397.3	396.5	396.4	-0.9	396.1	-0.4
<i>Planck</i> lensing	9.1	9.6	9.5	0.4	9.4	-0.2
BAO low-z	1.6	1.8	1.8	0.1	1.8	0.1
BAO high-z + $f\sigma_8$	5.9	–	6.8	0.9	–	–
EFTofLSS + BAO / CMASS NGC	–	65.9	–	–	67.1	1.3
EFTofLSS + BAO / CMASS SGC	–	61.9	–	–	63.0	1.1
EFTofLSS + BAO / LOWZ NGC	–	69.9	–	–	69.9	0.0
Pantheon	1,027.0	1026.9	1,027.3	0.3	1027.4	0.5
BBN	< 0.1	< 0.1	< 0.1	0.0	< 0.1	0.0
SH ₀ ES	17.1	16.2	3.3	-13.8	3.7	-12.5
$\chi^2(\text{total})$	3,829.6	4,022.5	3,814.0	–	4,007.8	–
$\Delta\chi^2(\text{total})$	–	–	–	-15.6	–	-14.7

TABLE II. The bestfit $\chi^2 = -2\ln(\mathcal{L})$ from combined analysis with and without EFTofLSS. The relative fit improvement is quantified through $\Delta\chi^2 = \chi^2(\text{NEDE}) - \chi^2(\Lambda\text{CDM})$.

to the standard Λ CDM parameters, the biggest change occurs for w_{cdm} , which decreases by 1% whereas the other Λ CDM parameters change by less than 0.3%. This had to be expected as w_{cdm} directly affects LSS parameters and hence is most constrained by the EFTofLSS. Moreover, decreasing w_{cdm} , while keeping the other parameters approximately constant, leads to a slight decrease in the σ_8 parameter, defined as the root-mean-square mass fluctuation in a sphere of radius 8 Mpc/h at $z = 0$. This in turn reduces $S_8 = \sigma_8\sqrt{\Omega_m/0.3}$ by 0.6% (the effect is attenuated by a slight drop in H_0). The phenomenological constraints are depicted as the light blue band in the last panel of Fig. 2 (we cite $S_8 = 0.762_{-0.024}^{+0.025}$ from a combined tomographic weak gravitational lensing analysis of the Kilo Degree Survey and the Dark Energy Survey [65]). We then find that the S_8 tension is still significant at 2.7σ (and 2.8σ without EFTofLSS). However, this has to be compared to a $\simeq 2.5$ tension within Λ CDM [26, 65] (without SH₀ES)⁸, which is only marginally lower.

⁸ Note that including SH₀ES lowers the tension within Λ CDM. This however is not a viable way of alleviating the problem as it relies on combining incompatible data sets.

This picture is confirmed by our χ^2 analysis in Tab. II. It shows that the overall χ^2 improvement is only slightly affected by including the EFTofLSS and amounts to $\Delta\chi^2(\text{total}) \simeq -15$. In this context, it is interesting to note that the Λ CDM fit to high- ℓ Planck data gets worse upon inclusion of the EFTofLSS data, which we believe is a manifestation of the LSS/ S_8 tension already present within Λ CDM at the $\simeq 2 - 3\sigma$ level [65, 66]. Within NEDE, on the other hand, that deterioration of the high- ℓ Planck fit can be completely avoided. We attribute this to the tendency of NEDE to give less power on small scales, which is a distinctive feature when comparing with its EDE competitors and Λ CDM (see Fig. 17 in [26]). This, however, comes at the price of worsening the fit to the EFTofLSS data set. Both effects – the improved fit to Planck and the worse fit to the full-shape data – compensate each other almost perfectly. In other words, the additional LSS data leads to a similar overall (negative) effect on both the Λ CDM and NEDE fit, which explains why it cannot significantly lower the evidence for NEDE.

IV. CONCLUSIONS

In this short note, we confronted NEDE with full-shape LSS data using the EFTofLSS applied to BOSS/SDSS in order to address recent concerns regarding the phenomenological viability of a class of EDE models. To that end, we used the publicly available code `PyBird`, which allowed us to implement the same data pipeline as the one used in [24] to constrain single-field EDE models. We report that adding the full-shape information has an insignificant effect on NEDE. In particular, we still find a rather high $\simeq 4\sigma$ evidence for a non-vanishing fraction of NEDE alongside $H_0 = 71.2 \pm 1.0 \text{ km s}^{-1} \text{ Mpc}^{-1}$ (68% C.L.), which is fully compatible with $H_0 = 71.4 \pm 1.0 \text{ km s}^{-1} \text{ Mpc}^{-1}$ (68% C.L.) obtained without full-shape data. In conclusion our model is consistent with current LSS data as implemented by `PyBird`.

However, it is also clear from our analysis that NEDE cannot improve on the tension with LSS data already present in Λ CDM. In particular, NEDE is 2.7σ discrepant with the value of S_8 , which is of a similar level as the tension within Λ CDM. There are two main conclusions we can reach from this. First, more LSS data, as it will be provided by future spectroscopic galaxy surveys such as Euclid [67] and the Dark Energy Spectroscopic Instrument [68], has the potential to confirm or rule out the base NEDE model as a resolution to the Hubble tension. A similar point was made in the

case of single-field EDE [23]. Second, further improvements of the current model should be guided by the aim to reduce the S_8 tension below its Λ CDM level. For different ideas how this can be achieved within NEDE see the corresponding discussion in [26].

ACKNOWLEDGMENTS

We thank Guido D’Amico for private correspondence, assistance in setting up the base Λ CDM run using PyBird and comments on the draft. We also thank the SDU eScience Center for providing us with the computational resources for the MCMC analysis. This work is supported by Villum Fonden grant 13384.

-
- [1] A. G. Riess, S. Casertano, W. Yuan, L. M. Macri, and D. Scolnic, *Astrophys. J.* **876**, 85 (2019), arXiv:1903.07603 [astro-ph.CO].
 - [2] K. C. Wong *et al.*, (2019), arXiv:1907.04869 [astro-ph.CO].
 - [3] N. Aghanim *et al.* (Planck), (2018), arXiv:1807.06209 [astro-ph.CO].
 - [4] J. L. Bernal, L. Verde, and A. G. Riess, *JCAP* **1610**, 019 (2016), arXiv:1607.05617 [astro-ph.CO].
 - [5] L. Knox and M. Millea, *Phys. Rev. D* **101**, 043533 (2020), arXiv:1908.03663 [astro-ph.CO].
 - [6] L. Verde, T. Treu, and A. Riess (2019) arXiv:1907.10625 [astro-ph.CO].
 - [7] A. G. Riess, *Nature Rev. Phys.* **2**, 10 (2019), arXiv:2001.03624 [astro-ph.CO].
 - [8] W. L. Freedman *et al.*, (2019), 10.3847/1538-4357/ab2f73, arXiv:1907.05922 [astro-ph.CO].
 - [9] W. L. Freedman, B. F. Madore, T. Hoyt, I. S. Jang, R. Beaton, M. G. Lee, A. Monson, J. Neeley, and J. Rich, (2020), 10.3847/1538-4357/ab7339, arXiv:2002.01550 [astro-ph.GA].
 - [10] K. Aylor, M. Joy, L. Knox, M. Millea, S. Raghunathan, and W. L. K. Wu, *Astrophys. J.* **874**, 4 (2019), arXiv:1811.00537 [astro-ph.CO].
 - [11] L. Verde, J. L. Bernal, A. F. Heavens, and R. Jimenez, *Mon. Not. Roy. Astron. Soc.* **467**, 731 (2017), arXiv:1607.05297 [astro-ph.CO].
 - [12] N. Arendse, A. Agnello, and R. Wojtak, *Astron. Astrophys.* **632**, A91 (2019), arXiv:1905.12000 [astro-ph.CO].
 - [13] V. Poulin, T. L. Smith, D. Grin, T. Karwal, and M. Kamionkowski, *Phys. Rev.* **D98**, 083525 (2018), arXiv:1806.10608 [astro-ph.CO].
 - [14] V. Poulin, T. L. Smith, T. Karwal, and M. Kamionkowski, *Phys. Rev. Lett.* **122**, 221301 (2019), arXiv:1811.04083 [astro-ph.CO].

- [15] T. L. Smith, V. Poulin, and M. A. Amin, *Phys. Rev. D* **101**, 063523 (2020), arXiv:1908.06995 [astro-ph.CO].
- [16] M.-X. Lin, G. Benevento, W. Hu, and M. Raveri, *Phys. Rev. D* **100**, 063542 (2019), arXiv:1905.12618 [astro-ph.CO].
- [17] N. Kaloper, *Int. J. Mod. Phys. D* **28**, 1944017 (2019), arXiv:1903.11676 [hep-th].
- [18] S. Alexander and E. McDonough, *Phys. Lett. B* **797**, 134830 (2019), arXiv:1904.08912 [astro-ph.CO].
- [19] E. Hardy and S. Parameswaran, *Phys. Rev. D* **101**, 023503 (2020), arXiv:1907.10141 [hep-th].
- [20] J. Sakstein and M. Trodden, *Phys. Rev. Lett.* **124**, 161301 (2020), arXiv:1911.11760 [astro-ph.CO].
- [21] M. Braglia, W. T. Emond, F. Finelli, A. E. Gumrukcuoglu, and K. Koyama, (2020), arXiv:2005.14053 [astro-ph.CO].
- [22] J. C. Hill, E. McDonough, M. W. Toomey, and S. Alexander, (2020), arXiv:2003.07355 [astro-ph.CO].
- [23] M. M. Ivanov, E. McDonough, J. C. Hill, M. Simonović, M. W. Toomey, S. Alexander, and M. Zaldarriaga, (2020), arXiv:2006.11235 [astro-ph.CO].
- [24] G. D’Amico, J. Gleyzes, N. Kokron, K. Markovic, L. Senatore, P. Zhang, F. Beutler, and H. Gil-Marn, *JCAP* **05**, 005 (2020), arXiv:1909.05271 [astro-ph.CO].
- [25] F. Niedermann and M. S. Sloth, (2019), arXiv:1910.10739 [astro-ph.CO].
- [26] F. Niedermann and M. S. Sloth, (2020), arXiv:2006.06686 [astro-ph.CO].
- [27] G. D’Amico, L. Senatore, P. Zhang, and H. Zheng, (2020), arXiv:2006.12420 [astro-ph.CO].
- [28] D. Baumann, A. Nicolis, L. Senatore, and M. Zaldarriaga, *JCAP* **07**, 051 (2012), arXiv:1004.2488 [astro-ph.CO].
- [29] J. J. M. Carrasco, M. P. Hertzberg, and L. Senatore, *JHEP* **09**, 082 (2012), arXiv:1206.2926 [astro-ph.CO].
- [30] R. A. Porto, L. Senatore, and M. Zaldarriaga, *JCAP* **05**, 022 (2014), arXiv:1311.2168 [astro-ph.CO].
- [31] J. J. M. Carrasco, S. Foreman, D. Green, and L. Senatore, *JCAP* **07**, 056 (2014), arXiv:1304.4946 [astro-ph.CO].
- [32] J. J. M. Carrasco, S. Foreman, D. Green, and L. Senatore, *JCAP* **07**, 057 (2014), arXiv:1310.0464 [astro-ph.CO].
- [33] S. M. Carroll, S. Leichenauer, and J. Pollack, *Phys. Rev. D* **90**, 023518 (2014), arXiv:1310.2920 [hep-th].
- [34] L. Senatore and M. Zaldarriaga, *JCAP* **02**, 013 (2015), arXiv:1404.5954 [astro-ph.CO].
- [35] T. Baldauf, E. Schaan, and M. Zaldarriaga, *JCAP* **03**, 007 (2016), arXiv:1507.02255 [astro-ph.CO].
- [36] S. Foreman, H. Perrier, and L. Senatore, *JCAP* **05**, 027 (2016), arXiv:1507.05326 [astro-ph.CO].
- [37] T. Baldauf, L. Mercolli, and M. Zaldarriaga, *Phys. Rev. D* **92**, 123007 (2015), arXiv:1507.02256 [astro-ph.CO].
- [38] M. Cataneo, S. Foreman, and L. Senatore, *JCAP* **04**, 026 (2017), arXiv:1606.03633 [astro-ph.CO].
- [39] M. Lewandowski and L. Senatore, *JCAP* **08**, 037 (2017), arXiv:1701.07012 [astro-ph.CO].

- [40] T. Konstandin, R. A. Porto, and H. Rubira, *JCAP* **11**, 027 (2019), arXiv:1906.00997 [astro-ph.CO].
- [41] E. Pajer and M. Zaldarriaga, *JCAP* **08**, 037 (2013), arXiv:1301.7182 [astro-ph.CO].
- [42] A. A. Abolhasani, M. Mirbabayi, and E. Pajer, *JCAP* **05**, 063 (2016), arXiv:1509.07886 [hep-th].
- [43] L. Mercolli and E. Pajer, *JCAP* **03**, 006 (2014), arXiv:1307.3220 [astro-ph.CO].
- [44] L. Senatore and M. Zaldarriaga, (2014), arXiv:1409.1225 [astro-ph.CO].
- [45] M. Lewandowski, A. Perko, and L. Senatore, *JCAP* **05**, 019 (2015), arXiv:1412.5049 [astro-ph.CO].
- [46] T. Baldauf, M. Mirbabayi, M. Simonović, and M. Zaldarriaga, *Phys. Rev. D* **92**, 043514 (2015), arXiv:1504.04366 [astro-ph.CO].
- [47] D. Blas, M. Garny, M. M. Ivanov, and S. Sibiryakov, *JCAP* **07**, 028 (2016), arXiv:1605.02149 [astro-ph.CO].
- [48] L. Senatore and G. Trevisan, *JCAP* **05**, 019 (2018), arXiv:1710.02178 [astro-ph.CO].
- [49] M. Lewandowski and L. Senatore, *JCAP* **03**, 018 (2020), arXiv:1810.11855 [astro-ph.CO].
- [50] M. M. Ivanov, M. Simonović, and M. Zaldarriaga, *JCAP* **05**, 042 (2020), arXiv:1909.05277 [astro-ph.CO].
- [51] T. Colas, G. D’amico, L. Senatore, P. Zhang, and F. Beutler, *JCAP* **06**, 001 (2020), arXiv:1909.07951 [astro-ph.CO].
- [52] G. D’Amico, L. Senatore, and P. Zhang, (2020), arXiv:2003.07956 [astro-ph.CO].
- [53] C.-P. Ma and E. Bertschinger, *Astrophys. J.* **455**, 7 (1995), arXiv:astro-ph/9506072 [astro-ph].
- [54] D. Blas, J. Lesgourgues, and T. Tram, *JCAP* **1107**, 034 (2011), arXiv:1104.2933 [astro-ph.CO].
- [55] B. Audren, J. Lesgourgues, K. Benabed, and S. Prunet, *JCAP* **1302**, 001 (2013), arXiv:1210.7183 [astro-ph.CO].
- [56] T. Brinckmann and J. Lesgourgues, (2018), arXiv:1804.07261 [astro-ph.CO].
- [57] W. Hu, *The Astrophysical Journal* **506**, 485494 (1998).
- [58] N. Aghanim *et al.* (Planck), (2019), arXiv:1907.12875 [astro-ph.CO].
- [59] D. M. Scolnic *et al.*, *Astrophys. J.* **859**, 101 (2018), arXiv:1710.00845 [astro-ph.CO].
- [60] E. Aver, K. A. Olive, and E. D. Skillman, *JCAP* **1507**, 011 (2015), arXiv:1503.08146 [astro-ph.CO].
- [61] A. J. Ross, L. Samushia, C. Howlett, W. J. Percival, A. Burden, and M. Manera, *Mon. Not. Roy. Astron. Soc.* **449**, 835 (2015), arXiv:1409.3242 [astro-ph.CO].
- [62] F. Beutler, C. Blake, M. Colless, D. H. Jones, L. Staveley-Smith, L. Campbell, Q. Parker, W. Saunders, and F. Watson, *Monthly Notices of the Royal Astronomical Society* **416**, 3017 (2011), <http://oup.prod.sis.lan/mnras/article-pdf/416/4/3017/2985042/mnras0416-3017.pdf>.
- [63] S. Alam *et al.* (BOSS), *Mon. Not. Roy. Astron. Soc.* **470**, 2617 (2017), arXiv:1607.03155 [astro-ph.CO].
- [64] A. Gelman and D. B. Rubin, *Statist. Sci.* **7**, 457 (1992).
- [65] S. Joudaki *et al.*, *Astron. Astrophys.* **638**, L1 (2020), arXiv:1906.09262 [astro-ph.CO].
- [66] M. Asgari *et al.*, *Astron. Astrophys.* **634**, A127 (2020), arXiv:1910.05336 [astro-ph.CO].

- [67] L. Amendola *et al.*, Living Rev. Rel. **21**, 2 (2018), arXiv:1606.00180 [astro-ph.CO].
- [68] M. E. Levi *et al.* (DESI), (2019), arXiv:1907.10688 [astro-ph.IM].